

See discussions, stats, and author profiles for this publication at: <https://www.researchgate.net/publication/263549542>

High-Angle Tilt Boundary Graphene Domain Recrystallized from Mobile Hot-Wire-Assisted Chemical Vapor Deposition System

ARTICLE in NANO LETTERS · JUNE 2014

Impact Factor: 13.59 · DOI: 10.1021/nl5012323 · Source: PubMed

CITATIONS

5

READS

50

11 AUTHORS, INCLUDING:



Gyeong Hee Ryu

Ulsan National Institute of Science and Techn...

21 PUBLICATIONS 81 CITATIONS

[SEE PROFILE](#)



Bo Hyun Kim

Korea Advanced Institute of Science and Tech...

22 PUBLICATIONS 530 CITATIONS

[SEE PROFILE](#)



Zonghoon Lee

Ulsan National Institute of Science and Techn...

105 PUBLICATIONS 2,516 CITATIONS

[SEE PROFILE](#)

High-Angle Tilt Boundary Graphene Domain Recrystallized from Mobile Hot-Wire-Assisted Chemical Vapor Deposition System

Jinsup Lee,^{†,⊥} Jinwook Baek,^{†,⊥} Gyeong Hee Ryu,[‡] Mi Jin Lee,[‡] Seran Oh,^{†,⊥} Seul Ki Hong,^{||,⊥} Bo-Hyun Kim,[†] Seok-Hee Lee,^{||} Byung Jin Cho,^{||,⊥} Zonghoon Lee,^{*,‡,§} and Seokwoo Jeon^{*,†,⊥}

[†]Department of Materials Science and Engineering, Korea Advanced Institute of Science & Technology (KAIST), Daejeon 305-701, Republic of Korea

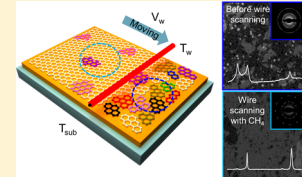
[‡]School of Materials Science and Engineering and [§]Low Dimensional Carbon Materials Center, Ulsan National Institute of Science and Technology (UNIST), Ulsan 689-798, Republic of Korea

^{||}Department of Electrical Engineering, Korea Advanced Institute of Science and Technology (KAIST), Daejeon 305-701, Republic of Korea

[⊥]Graphene Research Center and KI for NanoCentury, Korea Advanced Institute of Science & Technology, Daejeon 305-701, Republic of Korea

Supporting Information

ABSTRACT: Crystallization of materials has attracted research interest for a long time, and its mechanisms in three-dimensional materials have been well studied. However, crystallization of two-dimensional (2D) materials is yet to be challenged. Clarifying the dynamics underlying growth of 2D materials will provide the insight for the potential route to synthesize large and highly crystallized 2D domains with low defects. Here, we present the growth dynamics and recrystallization of 2D material graphene under a mobile hot-wire assisted chemical vapor deposition (MHW-CVD) system. Under local but sequential heating by MHW-CVD system, the initial nucleation of nanocrystalline graphenes, which was not extended into the growth stage due to the insufficient thermal energy, took a recrystallization and converted into a grand single crystal domain. During this process, the stitching-like healing of graphene was also observed. The local but sequential endowing thermal energy to nanocrystalline graphenes enabled us to simultaneously reveal the recrystallization and healing dynamics in graphene growth, which suggests an alternative route to synthesize a highly crystalline and large domain size graphene. Also, this recrystallization and healing of 2D nanocrystalline graphenes offers an interesting insight on the growth mechanism of 2D materials.



KEYWORDS: *graphene, recrystallization, high-angle tilt boundary, global domain, chemical vapor deposition*

In three-dimensional crystals, the average grain size and defect density of the crystal govern the mechanical and electrical properties of the materials, so a lot of work has been performed to realize low-defect, single-crystal growth. For example, the Czocharski method and floating-zone recrystallization have been known to purify substances and form single crystals for electrical grade of Si wafers.^{1–5} These methods have shown that the intrinsic properties of materials could be affected by alternation of the nucleation and growth mechanisms. Likewise, the mechanical and electrical properties of two-dimensional (2D) materials are significantly influenced by the grain size and number of boundaries.^{6–8} Therefore, systematic analysis of growth dynamics in 2D graphene is significant to provide the root to control the domain size and defect of graphene used for high performing electrical devices in the near future.^{6,9–14} Although the growth mechanism under the chemical vapor deposition (CVD) system has been actively studied in many previous works,^{15–17} there are still many obscurities of growth dynamics remaining to be proved. One of the key issues in graphene science is how to enlarge the grain size by reducing the number of grain boundaries. Recently, several groups have reported the synthesis of large graphene

domains of up to several millimeters by controlling partial pressure of hydrogen, regulating carbon feed gas, or varying carbon sources.^{12,13,18–22} However, simultaneous control of the nucleation sites and the growth behavior of graphene from the sites have only partial success from previous literature^{6,17,19} due to the difficulty in applying separate temperatures for nucleation and growth, respectively.

Here, we have discovered for the first time, the recrystallization-like behavior in 2D material graphene through mobile hot-wire (MHW)-assisted CVD. At the optimal temperature of hot-wire and substrate, graphene nanoclusters merged with other adjacent small-angle clusters to form a several hundred micron patch of global graphene domains which is a large crystalline graphene domain embedding high-angle tilt boundary (HATB) small graphene domains. The influence of the MHW at various speeds during the growth of the graphene is clearly indicated through Raman spectroscopy, electrical properties, and transmission electron microscopy

Received: April 2, 2014

Revised: May 23, 2014

Published: June 30, 2014

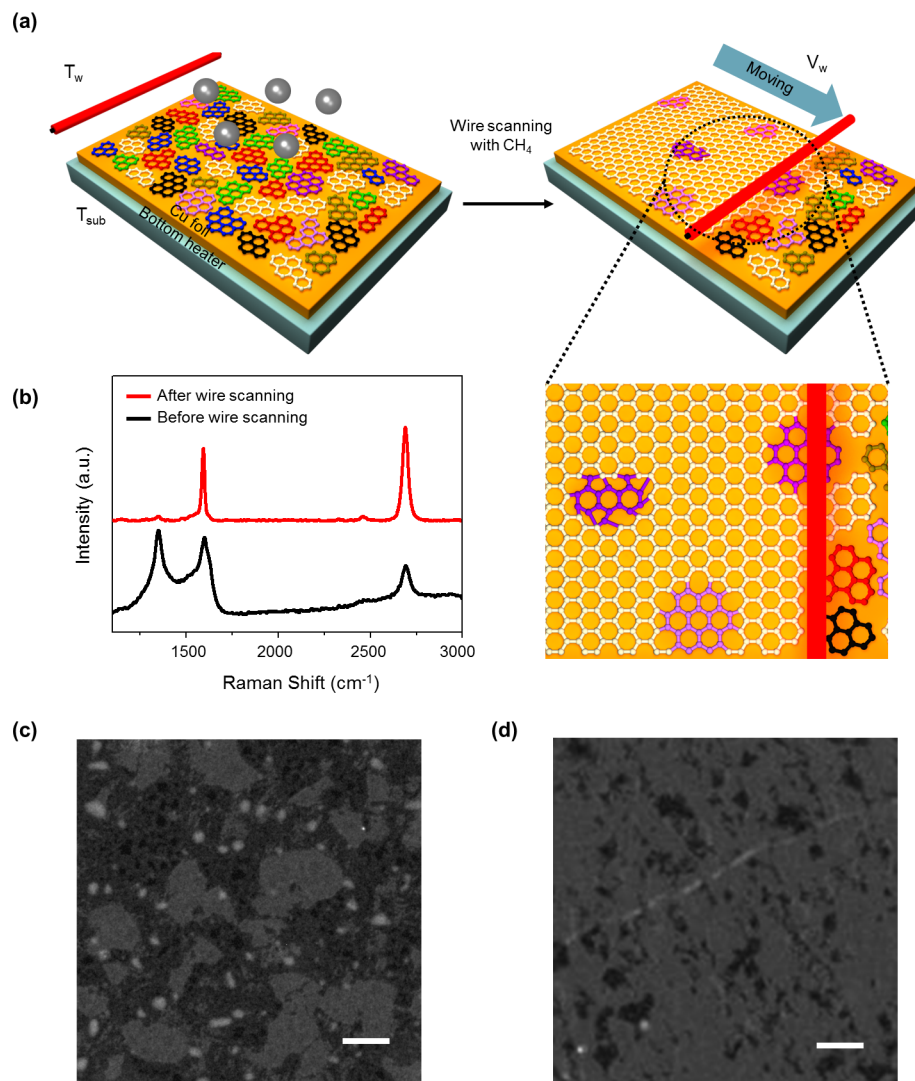


Figure 1. Synthetic method and spectroscopic analysis of graphene by MHW assisted CVD system. (a) Synthetic protocol of highly oriented graphene from nanocrystallized graphene. (b) Raman spectrum of before and after wire scanned over graphene. (c, d) DF TEM images (scale bar, 200 nm) of the as-grown graphene before (c) and after (d) wire scanning at T_{sub} of 820 °C.

(TEM).^{23–26} Two distinct growth experiments with/without a carbon source under the MHW provided an exclusive path to explore the adsorption/desorption kinetics of carbon in dynamic equilibrium state, in which could be simultaneously observed the healing of the defective sites of the graphene.

We have studied graphene nanoclusters nucleated on a surface that are consecutively growing, merging, and healing through controlling external variables including the substrate temperature (T_{sub}), wire scan speed (V_w), and carbon feedstock. Figure 1a presents the MHW assisted CVD system that was designed for controlling external variables in graphene synthesis. Unlike conventional CVD systems, our system has two independent heat sources; a floating mobile hot wire (1 mm diameter, Korea Tungsten Co.) supplying heat energy for cracking a carbon source and nucleating graphene nanoclusters, and a metal pedestal controlling T_{sub} from room temperature to 860 °C. These separated heat sources enabled us to control the formation and the growth of graphene through regulating the heating and cooling rate in a specific area. The effect of the hot-wire depends on the distance between the stationary wire and Cu foil, which is explained more elsewhere (Supporting Information Figure S1). While hot wire was on and laid

outside graphene growth area 15 cm apart, the preloading of carbon source into the chamber was made by the flow of CH_4 (5 sccm) and H_2 gas (200 sccm) above the hot-wire for 5 min. Even without the scanning of hot-wire, graphene nanoclusters and amorphous carbons (Figure 1a) were observed from the surface of Cu foil on a heated substrate (610–820 °C). The size of preformed graphene nanoclusters was maximum 0.1 μm at $T_{\text{sub}} = 820$ °C and they were randomly oriented. After preformed graphene nanoclusters, Cu foil was scanned by the hot-wire with a steady distance of 1 mm above the ground in varying V_w from 0.01 to 3.5 mm/min. While swiping, a mixture gas of H_2/CH_4 (200 sccm/5 sccm) was consistently injected without the change or interruption of the gas flow and substrate temperature from just above the hot-wire under vacuum at 5×10^{-3} Torr (see methods in the Supporting Information). This hot-wire swiping over the preformed graphene nanoclusters induced recrystallization into larger size graphene domains on the Cu foil. Surprisingly, this orientation of graphene domains gradually has specific angle with adjacent domains followed by increasing heat energy during the hot-wire's motion (Supporting Information Movie 1). The representative Raman spectra observed from substrate before and after wire scanning are

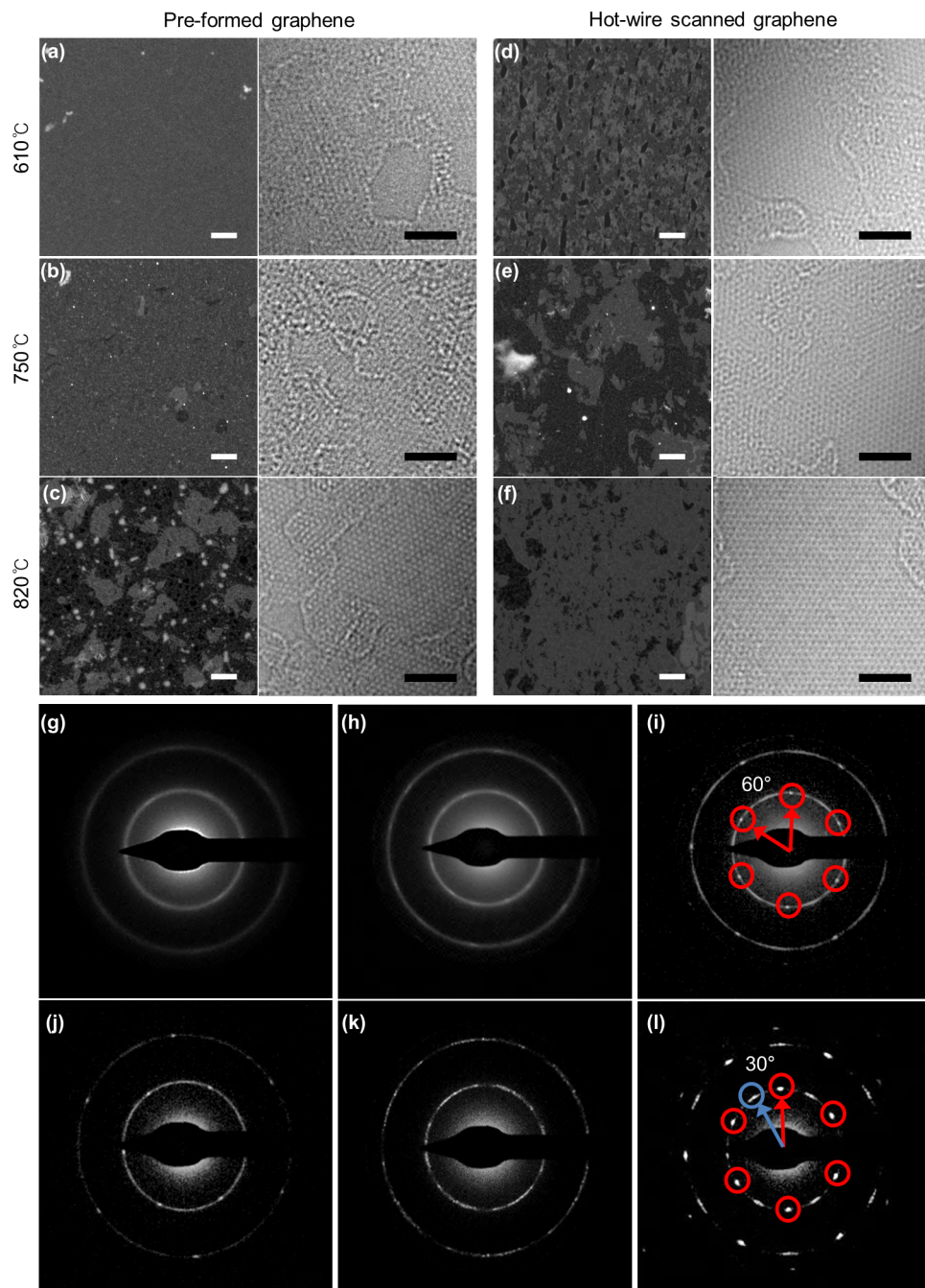


Figure 2. Observation of oriented, nanosized graphene domains after moving the hot-wire. (a–f) DF TEM images (left; scale bar, 200 nm) and high-resolution TEM images (right; scale bar, 2 nm) of the as-grown graphene before (a–c) and after (d–f) wire scanning at T_{sub} of 610 °C (a and d), 750 °C (b and e), and 820 °C (c and f). (g–l) Diffraction patterns of an as-grown graphene corresponding with DF TEM images in (a–f), respectively. The hot-wire is scanned from bottom to top during graphene growth. The red and blue circles in (i) and (l) indicate two types of first-order diffraction spots. In (i) and (l), red circles show single spots and the blue circle exhibits more than one conjugated spot having high-angles (almost 30°).

shown in Figure 1b. The decreasing Raman D peak suggests the reduced defect, whereas the sp^2 carbon structure increases along with the wire scanning. Likewise, the dark-field (DF) TEM images show the enlarged graphene domain after (Figure 1d) wire scanning compared to that before wire scanning (Figure 1c). Moreover, to further demonstrate the quality of graphene on large area, atomic force microscopy (AFM) and scanning electron microscopy (SEM) were used to surface morphology of as-grown graphene on Cu and transferred on SiO_2 substrate (Supporting Information Figure S2).

For the detail analysis of the enlargement of domain size under the hot-wire scanning, we performed the systematic studies by varying the substrate temperature and cooling rate. Figure 2 shows the comparison of DF TEM (Figure 2a–f, left), high-resolusion TEM image (Figure 2a–f, right) and diffraction patterns (Figure 2g–i) obtained from the preformed graphene with those from hot-wire scanned graphene according to the T_{sub} (610, 750, and 820 °C, respectively). Diffraction patterns correspond to DF TEM image, respectively. The average size of a nanocrystalline graphenes preformed at $T_{\text{sub}} = 610$ °C was

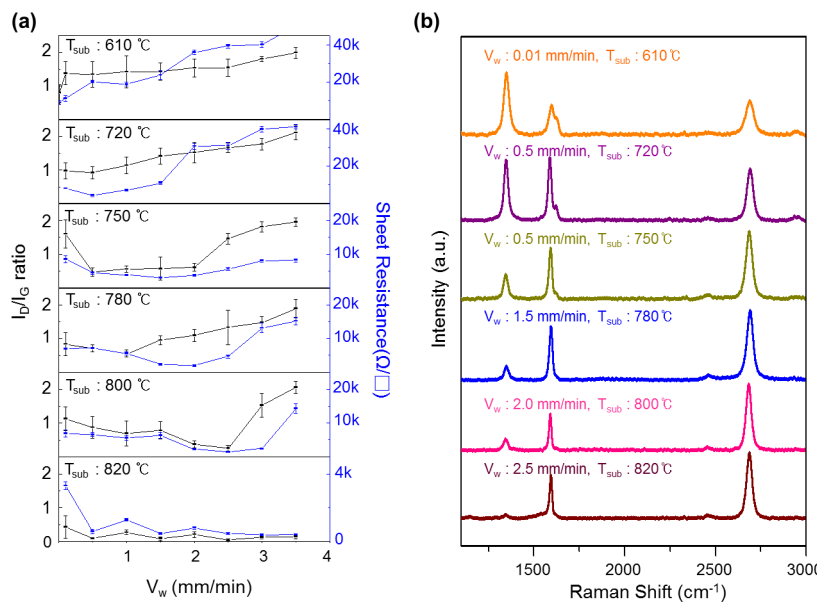


Figure 3. Effect of mobile wire and the correlation between the scan speed and electrical properties. (a) Graphene sheet resistance (blue) and I_D/I_G ratio (black) in the Raman spectra as a function of V_w with T_{sub} ranging from 610 to 820 °C. (b) Raman spectra of wire scanned as-grown graphene at the optimal scan speed shown the lowest sheet resistance with the indicated temperatures from 610 to 820 °C.

below ~ 10 nm, which were randomly aligned with many small holes (Figure 2a). This is precisely shown in the DF TEM image and diffraction pattern (Figure 2g). Both the size and quality of preformed nanocrystalline graphene domains are increased with T_{sub} (Figure 2b, c) and details are demonstrated in Supporting Information Figure S3. Moreover, considerably excessive amount of amorphous carbon was observed that is simultaneously deposited on the substrate, resulting a clear ring type of the electron diffraction patterns. On the contrary, after the hot-wire scanning, those nanocrystalline graphenes were enlarged and connected to each other, although many defects still remained (Figure 2c). As T_{sub} increased from 610 to 750 °C (Figure 2b), the size of preformed graphenes increased with the maximum size of 100 nm at 820 °C (Figure 2c). However, it is notable that they were still randomly deposited and not constructed the grand size of domain in spite of a slight 6-fold symmetry spots (red circles) in Figure 2i (details in Supporting Information Figure S4). On the other hand, the hot-wire scanned graphenes were not only grown into grand domains expanding the connection to the whole area but also became a defectless graphene (Figure 2d–f). At $T_{sub} \sim 820$ °C, the highly ordered and defect free like graphene was observed shown in Figure 2f, l, where, unlike the preformed graphene, a 6-fold symmetry was clearly observed in the diffraction pattern, suggesting that the adsorbates might have been dissociated after the subsequent wire scanning. Consequently, we observed two types of domain orientations were almost 30° apart (between red and blue circle). This alignment demonstrates that the hot-wire scanned graphene produced from our work will be composed of nearly high-angle boundary and have possibility to reduce domain boundaries. Also, this result provides that the preformed nanocrystalline graphenes were recrystallized into larger graphene domains and the thermal energy from the substrate was required to synthesize high-quality graphene together with the thermal active energy of carbon.

The observed cooling and growth rates of the graphene correlated with V_w are confirmed by Raman spectroscopy and sheet resistance measurements (Figure 3a). Data obtained from

both the I_D/I_G ratio and the sheet resistance demonstrates similar tendencies as functions of V_w at a given T_{sub} . From the measurements, the samples with the best V_w were those with the smallest I_D/I_G ratio, which was correlated with the lower sheet resistance values and justified our presumption that the highest quality graphene could be grown by modifying V_w in this system (Figure 3b). A representative T_{sub} value was chosen between 610 and 820 °C for the following reasons: When the T_{sub} was below 600 °C, the substrate temperature was too low to form nucleated graphene nanoclusters, and the T_{sub} was above 850 °C, the substrate temperature was too high to observe the effect of the MHW. At low T_{sub} (610 °C) values, the Raman I_D/I_G ratio of the graphene monotonically increased above 2 as V_w increased. To confirm Raman I_D/I_G ratio at 820 °C T_{sub} , additional detailed Raman spectra of graphene are shown in Supporting Information Figure S5. Interestingly, as the T_{sub} increased, the optimum V_w of the hot-wire with a minimized I_D/I_G ratio increased (0.5, 1, and 2.5 mm/min at $T_{sub} = 750, 780$, and 800 °C, respectively), which implies that optimal cooling rate (as V_w increases, the cooling rate increases at a given T_{sub}) is the key factor in achieving a low I_D/I_G ratio to synthesize high-quality graphene. At a given V_w , higher T_{sub} slows the cooling rate, rendering the fixation of a global graphene domain, which is difficult due to residual thermal energy, even after wire is removed from its point nearest the growth substrate, and promotes dynamic mobile carbon adsorption/desorption. The data provided in Figure 3a indicate that higher optimum V_w improves graphene quality. Given the optimum V_w values at different T_{sub} values, a slower optimum V_w indicates an extended stay at the growth location under a constant carbon source influx, leading to an excess of carbon and an extended period of dynamic carbon adsorption/desorption, which explains why the lowest sheet resistance and I_D/I_G ratio were found from the $T_{sub} = 820$ °C samples ($390 \Omega/\square$ with $0.05 I_D/I_G$ at $V_w = 2.5$ mm/min). The improved uniformity of the 2D Raman mapping of the I_D/I_G and I_{2D}/I_G ratios from the samples at optimized T_{sub} can be

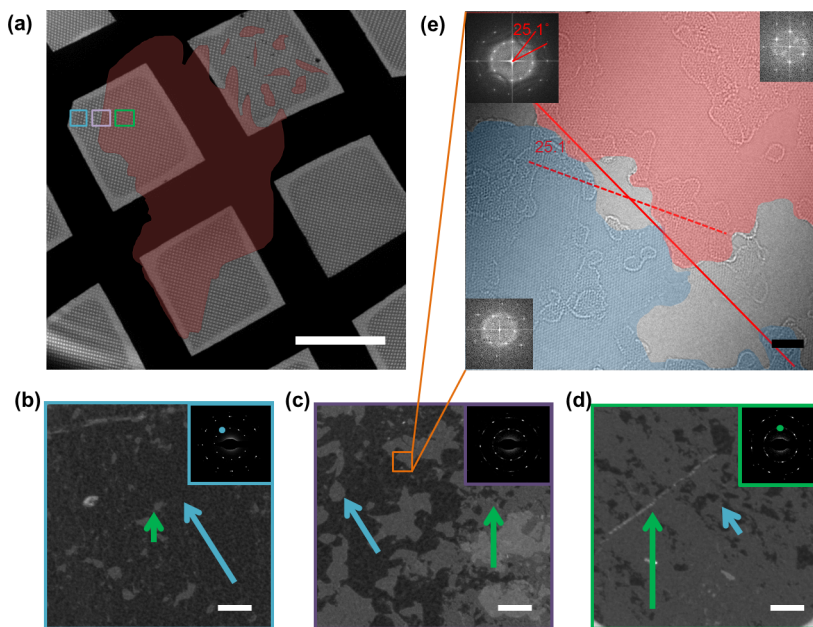


Figure 4. Domain characterization. (a) TEM domain mapping of wire-scanned graphene on the TEM grid with a boundary of same domain angle (red). Scale bar, 100 μm . (b–d) DF TEM image of the position marked by the cyan, pink and green squares in (a), respectively. Scale bar, 200 nm. The inset in each image presents the corresponding diffraction patterns. These DF images and diffraction patterns indicate the coincident contrast for the outside (b), inside (d), and boundary region (c) of the global graphene domains. The cyan circle and arrow (the inset in b) indicate one type of graphene domain angle and the blue circle and arrow (the inset in d) shows the other type of graphene domain angle with almost 30° high angle. (e) High-resolution TEM image of the boundary at the orange box in (c). This domain boundary (between the blue and red regions) retains a high-angle boundary (25.1°) with the diffraction pattern inset. Scale bar, 2 nm. This image exhibits disconnected domain boundaries (gray region in e). Thus, this measurement process produces many defects by exposing the focused beam despite the short exposure time due to the unstable state at the domain boundaries.

correlated with the improved sheet resistance at the optimal V_w (Supporting Information Figure S6).

The effects of the hot-wire on graphene growth are further analyzed via well-controlled experiments (Supporting Information Figure S7). The hot-wire was immobilized outside the copper foil (15 cm apart). The Raman peaks at 1349 cm^{-1} (D peak), 1594 cm^{-1} (G peak), and 2692 cm^{-1} (2D peak) do not appear when either the wire or metal substrate is not heated. When the hot-wire is off, no Raman signals for graphitic carbon appear up to $T_{\text{sub}} = 850$ °C. On a cold (<30 °C) substrate, even turning the hot-wire ($T_w = 1230$ °C) on could decompose the carbon sources supplied to the substrate; the decomposed carbon is not provided with sufficient thermal energy to form graphitic nanoclusters on the substrate (Supporting Information Figure S7). However, when T_{sub} is 610 °C while the hot-wire is on, a weak Raman signal for graphene appears and confirms that the precracking of the carbon source by the hot-wire effectively lowers the growth temperature of the substrate from 880 to 610 °C. After increasing T_{sub} from 610 to 820 °C, the intensity of the peaks increased and a 2D graphene peak appeared (purple, cyan, and navy respectively). Overall, the Raman signals of these samples (Supporting Information Figure S7b) are in sharp contrast to those from the samples that experienced the hot-wire scanning (Figure 3b). The Raman peak becomes sharp and distinct at optimized V_w values. As explained in Figure 2, the changing Raman signals result from the rearrangements of the nanocluster domains to form a global graphene domain. Moreover, this observation supports the need to optimize the temperature to create a high-quality single-layer graphene sheet with suitable V_w and T_{sub} values (from orange to brown).

We utilized TEM to investigate the characteristics of the highest quality graphene grown in our work ($T_{\text{sub}} = 820$ °C and $V_w = 2.5$ mm/min) (Figure 4). Figure 4a provides a domain map of a large area of the scanned high-quality graphene using a DF TEM mapping technique to encompass multiple domains. The mapping technique can accumulate and distinguish various domain boundaries by tracing the diffraction pattern transitions.²⁴ We were able to determine the extensive domain as indicated in the red area of Figure 4a up to a diagonal length of 323 μm : global domain. Unlike traditional graphene domain, global domain shows an unusual domain boundary and angle. As highlighted in Figure 4a, the cyan, violet and green boxes correspond to Figure 4b, c, and d, respectively. These images show the transition of the domain boundary via diffraction patterns. Figure 4b depicts the outside of a large domain using a dominant dark contrast, indicating that the crystallographic domains are oriented almost identically (cyan arrow). In this dark gray region, some embedded small regions with a bright gray represent another domain angle (green arrow). The inset provides the diffraction pattern of the image, which includes two dominant domain angles from the two sets of 6-fold symmetry at the diffraction spots with 30° angle (cyan circle). However, in Figure 4d, the bright contrast primarily represents the main domain angle related to the green circle in the diffraction pattern. This reverse color scheme in Figure 4d also corresponds to inverse diffraction pattern in inset of Figure 4d compared to that of Figure 4b. At the domain boundary region in Figure 4c, the two dominant domain angles confirmed in Figure 4b and d are measured using the distinct diffraction pattern. Moreover, the diffraction spots are also found with similar brightness, which demonstrate that the quantity of two dominant domain angles is almost same and the boundary of

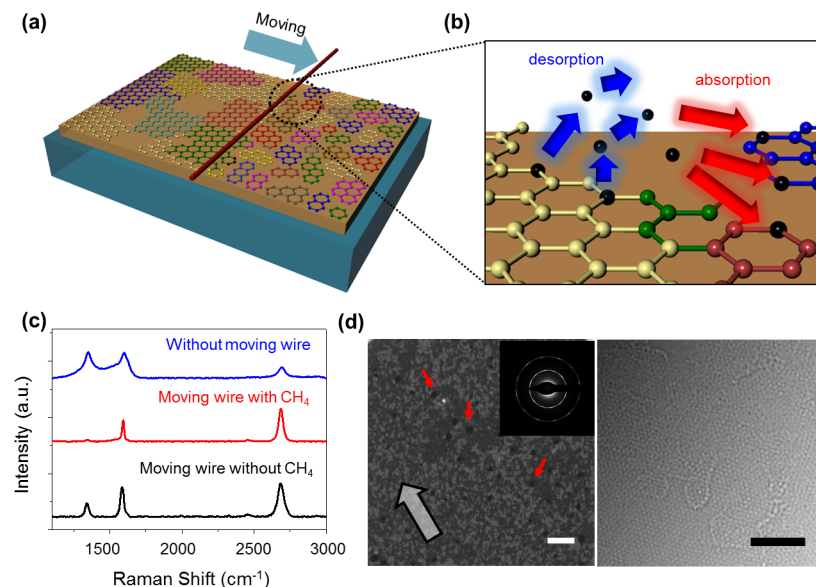


Figure 5. Recrystallization and healing of scanned graphene. (a) Diagrams of the wire-scanning process without a carbon source during wire moving. (b) Detailed schematic illustration of the thermal vibration of carbon under the wire in (a) with carbon adsorption and desorption. (c) Raman spectra of the graphene derived from the scanned wire, the stopped wire and the scanned wire without an additional carbon source. (d) DF TEM images (left; scale bar, 200 nm), diffraction patterns (left inset), and high-resolution TEM images (right; scale bar, 2 nm) of the as-grown graphene without an additional carbon source at $T_{\text{sub}} = 820^{\circ}\text{C}$. The arrow indicates the scanning direction of the hot-wire.

global domain exist as shown in Figure 4c. To confirm the domain boundary in global domain more clearly, we measured the bright-colored DF image at Figure 4c with changing TEM aperture angles (Supporting Information Figure S8). The orange box in Figure 4c indicates the imaging area that corresponds to Figure 4e, and the blue and red representative digital diffractograms overlaid on the global graphene domains yield a HATB of approximately 30° (more precisely saying 25.1°). Interestingly, this graphene describes only two types of global graphene domain angles without any other low-angle domains, indicating that low-angle domains are transformed into the dominant orientation or a high-angle tilt (HAT) domain during the wire scanning. Even though it remains unclear why domain boundary in our work mostly exhibit HAT domain, some previous reports represent statistical preference of misorientation angle distribution including $28\text{--}30^{\circ}$ in conventional CVD graphene.^{27–33} Moreover, in the previous theoretical studies, the grain boundary energy γ shows the lowest energy or an energy dip at $28\text{--}30^{\circ}$ tilt angle with pentagons “5” and heptagons “7” defect positions. In this respect, we can suggest one possible hypothesis. To reduce the grain boundary energy, the small domains representing high angle ($25\text{--}30^{\circ}$) remain as HATB islands in a large ($\sim 323 \mu\text{m}$) global domain where most other randomly oriented small domains (low angle $<20^{\circ}$) are consolidated into a larger single domain by recrystallization. This finding confirms the recrystallization in the wire-scanned graphene. Moreover, Supporting Information Figure S9 depicts many small isolated domains with one HAT that are embedded in the other large dominant domain, or global graphene domain, indicating that one global graphene domain contains many smaller isolated domains with the crystallographic orientation of the other global graphene domains. Additional images of the domain boundary transitions in Figure 4a are presented in Supporting Information Figure S10, which demonstrates that even remotely embedded small domains in one large global graphene domain consistently maintain the orientation of the other

global graphene domain. These recrystallized global graphene domains appear to have only two types of domain orientations—one from the main orientation, which is expressed in the large number of small domains in the domain map, and the other from the HAT small domains found within the main domain. These propagations with enlarged domain sizes can explain the recrystallization of graphene using a MHW assisted system. Furthermore, this incubation system composed of a global graphene domain and an internal HAT domain has not previously been demonstrated in a single graphene domain. For comparison, most single-layer polycrystalline graphene fabricated via CVD are reported to have only randomly oriented domains due to their finite growth mechanism, such as the formation of nucleation sites and subsequent growth, whereas in our results, the recrystallization mechanism is considered to be complementary with the typical global domain arising from directional graphene growth.

Well-designed graphene growth experiments with/without carbon feed gas provides additional insight into the dynamic adsorption/desorption behavior during the growth of global graphene domains. We probed the change in graphene growth behavior (Figure 5a) using the same experimental conditions without a CH_4 flow at the optimal sample of $T_{\text{sub}} = 820^{\circ}\text{C}$, as shown in Figure 2e and f. After 10 min of initial carbon cracking with the hot-wire to deposit carbon nanoclusters and 10 min of vacuuming by injecting pure Ar gas, the only carbon source is the predeposited graphitic nanoclusters. A detailed scheme presenting the moving carbon atom under the mobile wire is provided in Figure 5b (with Supporting Information Movie 2). This source restriction could interrupt the mode of graphene growth, such as cluster rotation, or the recrystallization-like stitching that is essential for growing a global graphene domain. Figure 5c and d exhibit an interesting difference between the samples with and without methane. The graphene sample grown without methane has a significantly increased Raman D peak (Figure 5c, black line) compared to the sample with the carbon source (Figure 5c, red line), but the samples

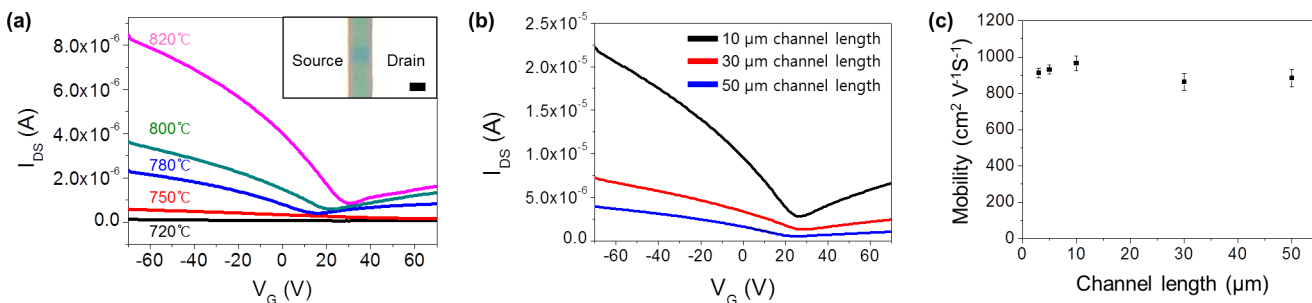


Figure 6. Electronic properties. (a) Transfer curve of the graphene FET for various T_{sub} values. The inset shows the graphene position and an effective channel length and width (blue line). The scale bar in inset represents 2 μm . (b) Transfer curve of the graphene FET for various channel length values. (c) FET mobility with various channel lengths.

still exhibit vast improvements over those without hot-wire motion (Figure 5c, blue line). This result confirms the healing action of the graphene with the hot-wire motion. Furthermore, the TEM image reveals an interesting morphology and structure of the graphene without CH_4 . Compared to Figure 2f, the TEM image in Figure 5d depicts numerous nanoholes (red arrow) that are direct evidence of a carbon deficiency during the recrystallization of graphene. Without an additional carbon source, the adsorption of carbon during the recrystallization from predeposited nanoclusters and the desorption of nanoclusters during the wire motion create samples with a large number of nanoholes. The inset in Figure 5d and Supporting Information Figure S11 also confirm the change in the graphene growth mode. The DF diffraction split of the large-angle boundary is less discrete than that found in the inset of Figure 2f, which could be due to the weak action of the cluster rotation during recrystallization. The insufficient rotation of small angled clusters due to a carbon deficiency can scatter the electron diffraction spots on the graphene domain. From this result, we indicate that the dynamic adsorption/desorption of carbon is crucial for the reconstruction, or healing, of graphene and that a carbon deficiency actively affects the growth or recrystallization of the graphene.

To evaluate the electrical characteristics of the wire-scanned graphene, we fabricated a back-gate field-effect transistor (FET) on a 100 nm Si/SiO₂ substrate (Figure 6). The devices were fabricated via photolithography and the isolation of graphene using Au (50 nm)/Pd (5 nm) source and drain electrodes. The channel length and width were 5–50 and 2 μm , respectively. The optimum graphene samples with the lowest I_D/I_G ratio in their Raman spectra at a given T_{sub} were selected to further investigate the transport properties. Given the as-determined sheet resistance value, the hole mobility of the optimized graphene samples increased with T_{sub} (the transport characteristic could not be measured for the $T_{\text{sub}} = 610$ °C sample because it was a discrete graphene sheet). Moreover, the correlation between an increased hole mobility, a reduced sheet resistance, and the I_D/I_G ratio from the Raman spectra confirms the hot-wire's role during growth. The highest hole mobility was measured in the graphene grown at $T_{\text{sub}} = 820$ °C is ~930 $\text{cm}^2 \text{V}^{-1} \text{s}^{-1}$ (Figure 6a) with a positive Dirac point (30 V), which is similar to or slightly lower than those measured from CVD graphene grown on Cu and then transferred to SiO₂.^{16,26} The value is reasonable considering the presence of HATBs in our samples. To determine the uniformity of graphene with global domain, similarly, we measured the hole mobility at long-range order (channel length is up to 50 μm), and representative plots are shown in Figure 6b and c. These

measurements show that our graphene might be homogeneously covered by similar global graphene domain structure.

In this work, we report a detailed growth mechanism for single-layer graphene with dominantly oriented global graphene domains by using a MHW assisted system. Our results indicate that graphene nanoclusters can be realigned to form a HATB. This phenomenon includes the nucleation of graphitic nanoclusters, subsequent growth, and a recrystallization-like stitching and rotation of small graphene domains. In particular, the synthesized global graphene domain has a HATB against the adjacent global graphene domain, and each global graphene domain has trapped nanosized inner domains, which retain one of the two global domain orientations. The controlled synthesis of graphene using this new CVD system with a MHW, which introduces directional cooling and a growth rate associated with the wire scan speed with a controlled substrate temperature and carbon source, enables a close investigation of this unusual growth mechanism of graphene, including the recrystallization-like growth and dynamic healing effect on the graphitic network. Thus, we believe our report offers a significant contribution to understanding the growth mechanism of graphene and enhancing the properties of CVD grown graphene by manipulating the nucleation and sequential growth.

ASSOCIATED CONTENT

Supporting Information

Experimental details such as graphene growth and transfer methods and analysis tools. Additional graphene characterization data including Raman spectra, DF TEM image, and diffraction pattern result. This material is available free of charge via the Internet at <http://pubs.acs.org>.

AUTHOR INFORMATION

Corresponding Authors

*E-mail: zhlee@unist.ac.kr.

*E-mail: jeon39@kaist.ac.kr.

Author Contributions

S.J. conceived the idea and developed the hot wire system. S.J. and Z.L. designed models and experiments to analyze the grown samples and J.L., J.B., B.K., and S.O. synthesized the samples and carried out the Raman spectra and resistance characterization. G.H.R. and M.J.L. performed TEM analysis, and S.H., S.L., and B.J.C. handled an electrical property measurement. S.J. and Z.L. supervised the project. All authors contributed to the discussions and wrote the manuscript.

Notes

The authors declare no competing financial interest.

ACKNOWLEDGMENTS

This work was supported by the Converging Research Center Program through the National Research Foundation of Korea (NRF) funded by the Ministry of Education, Science and Technology (2011K000623), and KAIST Institute for the NanoCentury in Korea. It was also partially supported by a grant (2011-0031630) from the Center for Advanced Soft Electronics under the Global Frontier Research Program of the Ministry of Education, Science and Technology, Korea. This research was partially supported by Nano-Material Technology Development Program through the National Research Foundation of Korea (NRF) funded by the Ministry of Science, ICT and Future Planning (2012M3A7B4049807).

REFERENCES

- (1) Baker, I.; Li, J. *Acta Mater.* **2002**, *50*, 805–813.
- (2) Takagi, K.; Ishii, M. *J. Mater. Sci.* **1977**, *12*, 517–521.
- (3) Badwal, S. P. S. *J. Mater. Sci.* **1984**, *19*, 1767–1776.
- (4) Pena, J. I.; Merino, R. I.; de la Fuente, G. F.; Orera, V. M. *Adv. Mater.* **1996**, *8*, 909–912.
- (5) Sumino, K.; Harada, H.; Yonenaga, I. *Jpn. J. Appl. Phys.* **1980**, *19*, L49–L52.
- (6) Yu, Q. K.; Jauregui, L. A.; Wu, W.; Colby, R.; Tian, J.; Su, Z.; Cao, H.; Liu, Z.; Pandey, D.; Wei, D.; Chung, T. F.; Peng, P.; Guisinger, N. P.; Stach, E. A.; Bao, J.; Pei, S.; Chen, Y. P. *Nat. Mater.* **2011**, *10*, 443–449.
- (7) Tsien, A. W.; Brown, L.; Levendorf, M. P.; Ghahari, F.; Huang, P. Y.; Havener, R. W.; Ruiz-Vargas, C. S.; Muller, D. A.; Kim, P.; Park, J. *Science* **2012**, *336*, 1143–1146.
- (8) Lee, G.; Cooper, R. C.; An, S. J.; Lee, S.; van der Zande, A.; Petrone, N.; Hammerberg, A. G.; Lee, C.; Crawford, B.; Oliver, W.; Kysar, J. W.; Hone, J. *Science* **2013**, *340*, 1073–1076.
- (9) Kwak, J.; Chu, J. H.; Choi, J.; Park, S.; Go, H.; Kim, S. Y.; Park, K.; Kim, Y.; Yoon, E.; Kodambaka, S.; Kwon, S. *Nat. Commun.* **2012**, *3*, 645 DOI: 10.1038/ncomms1650.
- (10) Kim, H.; Mattevi, C.; Calvo, M. R.; Oberg, J. C.; Artiglia, L.; Agnoli, S.; Hirjibehedin, C. F.; Chhowalla, M.; Saiz, E. *ACS Nano* **2012**, *6*, 3614–3623.
- (11) Celebi, K.; Cole, M. T.; Choi, J. W.; Wyczisk, F.; Legagneux, P.; Rupesinghe, N.; Robertson, J.; Teo, K. B. K.; Park, H. G. *Nano Lett.* **2013**, *13*, 967–974.
- (12) Vlassiouk, I.; Regmi, M.; Fulvio, P.; Dai, S.; Datskos, P.; Eres, G.; Smirnov, S. *ACS Nano* **2011**, *5*, 6069–6076.
- (13) Gao, L. B.; Ren, W. C.; Xu, H. L.; Jin, L.; Wang, Z. X.; Ma, T.; Ma, L. P.; Zhang, Z. Y.; Fu, Q.; Peng, L. M.; Bao, X. H.; Cheng, H. M. *Nat. Commun.* **2012**, *3*, 699 DOI: 10.1038/ncomms1702.
- (14) Wu, Y. M. A.; Fan, Y.; Speller, S.; Creeth, G. L.; Sadowski, J. T.; He, K.; Robertson, A. W.; Allen, C. S.; Warner, J. H. *ACS Nano* **2012**, *6*, 5010–5017.
- (15) Yu, Q. K.; Lian, J.; Siriponglert, S.; Li, H.; Chen, Y. P.; Pei, S. S. *Appl. Phys. Lett.* **2008**, *93*, 113103.
- (16) Li, X. S.; Magnuson, C. W.; Venugopal, A.; An, J. H.; Suk, J. W.; Han, B. Y.; Borysiak, M.; Cai, W. W.; Velamakanni, A.; Zhu, Y. W.; Fu, L. F.; Vogel, E. M.; Voelkl, E.; Colombo, L.; Ruoff, R. S. *Nano Lett.* **2010**, *10*, 4328–4334.
- (17) Bhaviripudi, S.; Jia, X. T.; Dresselhaus, M. S.; Kong, J. *Nano Lett.* **2010**, *10*, 4128–4133.
- (18) Zhou, H.; Yu, W. J.; Liu, L.; Cheng, R.; Chen, Y.; Huang, X.; Liu, Y.; Wang, Y.; Huang, Y.; Duan, X. *Nat. Commun.* **2013**, *4*, 2096 DOI: 10.1038/ncomms3096.
- (19) Wu, T. R.; Ding, G. Q.; Shen, H. L.; Wang, H. M.; Sun, L.; Jiang, D.; Xie, X. M.; Jiang, M. H. *Adv. Funct. Mater.* **2013**, *23*, 198–203.
- (20) Wang, H.; Wang, G. Z.; Bao, P. F.; Yang, S. L.; Zhu, W.; Xie, X.; Zhang, W. J. *J. Am. Chem. Soc.* **2012**, *134*, 3627–3630.
- (21) Chen, S. S.; Ji, H. X.; Chou, H.; Li, Q. Y.; Li, H. Y.; Suk, J. W.; Piner, R.; Liao, L.; Cai, W. W.; Ruoff, R. S. *Adv. Mater.* **2013**, *25*, 2062–2065.
- (22) Yan, Z.; Lin, J.; Peng, Z. W.; Sun, Z. Z.; Zhu, Y.; Li, L.; Xiang, C. S.; Samuel, E. L.; Kittrell, C.; Tour, J. M. *ACS Nano* **2012**, *6*, 9110–9117.
- (23) Huang, P. Y.; Ruiz-Vargas, C. S.; van der Zande, A. M.; Whitney, W. S.; Levendorf, M. P.; Kevek, J. W.; Garg, S.; Alden, J. S.; Hustedt, C. J.; Zhu, Y.; Park, J.; McEuen, P. L.; Muller, D. A. *Nature* **2011**, *469*, 389–392.
- (24) Kim, K.; Lee, Z.; Regan, W.; Kisielowski, C.; Crommie, M. F.; Zettl, A. *ACS Nano* **2011**, *5*, 2142–2146.
- (25) Li, X. S.; Cai, W. W.; An, J. H.; Kim, S.; Nah, J.; Yang, D. X.; Piner, R.; Velamakanni, A.; Jung, I.; Tutuc, E.; Banerjee, S. K.; Colombo, L.; Ruoff, R. S. *Science* **2009**, *324*, 1312–1314.
- (26) Kim, K. S.; Zhao, Y.; Jang, H.; Lee, S. Y.; Kim, J. M.; Kim, K. S.; Ahn, J. H.; Kim, P.; Choi, J. Y.; Hong, B. H. *Nature* **2009**, *457*, 706–710.
- (27) An, J. H.; Voelkl, E.; Suk, J. W.; Li, X. S.; Magnuson, C. W.; Fu, L. F.; Tiemeijer, P.; Bischoff, M.; Freitag, B.; Popova, E.; Ruoff, R. S. *ACS Nano* **2011**, *5*, 2433–2439.
- (28) Grantab, R.; Shenoy, V. B.; Ruoff, R. S. *Science* **2010**, *330*, 946–948.
- (29) Liu, Y. Y.; Yakobson, B. I. *Nano Lett.* **2010**, *10*, 2178–2183.
- (30) Yazyev, O. V.; Louie, S. G. *Phys. Rev. B: Condens. Matter Mater. Phys.* **2010**, *81*, 195420.
- (31) Malola, S.; Hakkinen, H.; Koskinen, P. *Phys. Rev. B: Condens. Matter Mater. Phys.* **2010**, *81*, 165447.
- (32) Yazyev, O. V.; Louie, S. G. *Nat. Mater.* **2010**, *9*, 806–809.
- (33) Yakobson, B. I.; Ding, F. *ACS Nano* **2011**, *5*, 1569–1574.